Spectroscopic and Computational Investigation of Low-Spin Mn(III) Bis(scorpionate) Complexes£

Hannah E. Colmer^, **Charles G. Margarit**†, **Jeremy M. Smith**†,§, **Timothy A. Jackson**^, and **Joshua Telser**‡

^Department of Chemistry, University of Kansas, Lawrence, Kansas 66045 USA

†Department of Chemistry and Biochemistry, New Mexico State University, Las Cruces, New Mexico 88003 USA

§Department of Chemistry, Indiana University, Bloomington, Indiana 47405 USA

‡Department of Biological, Chemical and Physical Sciences, Roosevelt University, Chicago, Illinois 60605 USA

Abstract

Six-coordinate Mn^{III} complexes are typically high-spin ($S = 2$), however, the scorpionate ligand, both in its traditional, hydridotris(pyrazolyl)borate form, Tp^- and Tp^{*-} (the latter with 3,5-dimethylpyrazole substituents) and in an aryltris(carbene)borate (*i.e.*, *N*-heterocyclic carbene, NHC) form, $[Ph(MeIm)_3B]^-$, (MeIm = 3-methylimidazole) lead to formation of bis(scorpionate) complexes of Mn^{III} with spin triplet ground states; three of which were investigated herein: $[Tp_2Mn]SbF_6$ (**1SbF$_6$**), $[Tp^*_2Mn]SbF_6$ (**2SbF$_6$**), and $[\{Ph(MeIm)_3B\}_2Mn]CF_3SO_3$ (**3CF$_3$SO$_3$**). These trigonally symmetric complexes were studied experimentally by magnetic circular dichroism (MCD) spectroscopy (the propensity of **3** to oxidize to Mn^{IV} precluded collection of useful MCD data) including variable temperatures and fields (VTVH-MCD) and computationally by ab initio CASSCF/NEVPT2 methods. These combined experimental and theoretical techniques establish the $^3A_{2g}$ electronic ground state for the three complexes, and provide information on the energy of the "conventional" high-spin excited state (^5E_g) and other, triplet excited states. These results show the electronic effect of pyrazole ring substituents in comparing **1** and **2**. The tunability of the scorpionate ligand, even by perhaps the simplest change (from pyrazole in **1** to 3,5-dimethylpyrazole in **2**) is quantitatively manifested through perturbations in ligand-field excited-state energies that impact ground-state zero-field splittings. The comparison with the NHC donor is much more dramatic. In **3**, the stronger σ-donor properties of the NHC lead to a quantitatively different electronic structure, so that the lowest lying spin triplet excited state, ^3E_g,

is much closer in energy to the ground state than in **1** or **2**. The zero-field splitting (zfs) parameters of the three complexes were calculated and in the case of **1** and **2** compare closely to experiment (lower by < 10%, < 2 cm^{-1} in absolute terms); for **3** the large magnitude zfs is reproduced, although there is ambiguity about its sign. The comprehensive picture obtained for these bis(scorpionate) Mn^{III} complexes provides quantitative insight into the role played by the scorpionate ligand in stabilizing unusual electronic structures.

Keywords

INTRODUCTION

Manganese complexes supported by "scorpionate" ligands, specifically derivatives of the hydridotris(pyrazolyl)borate anion (Tp$^-$), have been used to model intermediates formed in Mn-dependent enzymes.[1] These applications have featured Tp$^-$ ligands containing pyrazole groups modified with bulky isopropyl or phenyl substituents in the 3- and 5-positions. Such studies have also featured Mn^{II} and Mn^{III} ions in the expected high-spin states (S = 5/2 and S = 2, respectively). In contrast, the homoleptic Mn^{III} complexes supported by the Tp$^-$ and Tp*$^-$ ligands (Figure 1; Tp*$^-$ = hydridotris(3,5-dimethylpyrazolyl)borate) both possess an S = 1 spin state, which is extremely unusual for Mn^{III} centers.[2] Other than the hexacyanido complex, [Mn^{III}(CN)$_6$]$^{3-}$,[3] the "classic" example of coordination favoring low-spin ground states, there are very few examples of Mn^{III} coordination complexes with S = 1 ground states. These include an interesting class of complexes with a *cis*-N4O2 donor set (oximato-N, azo-N, and carboxylato-O), such as bis[((2-carboxylatophenyl)azo)benzaldoximato]manganate(III).[4] A related class of complexes is the tris(quinine oximates), with *mer*- and *fac*-O3N3 donor sets.[5] Other, perhaps more expected examples of low-spin Mn(III) are the porphyrin complexes [Mn(TPP)(CN)$_2$]$^-$,[6] and [Mn(TPP)(Im)$_2$]$^-$, where TPP = tetraphenylporphyrin dianion, Im = imidalozate anion,[7] and a saturated macrocyclic analog, [Mn(cyclam)(CN)$_2$]$^+$ (cyclam = 1,4,8,11-tetraazacyclotetradecane).[8]

Related to the above trispyrazolylborate complexes is the [{Ph(MeIm)$_3$B}$_2$Mn^{III}]$^+$ complex (Figure 1), where PhB(MeIm)$_3^-$ (phenyltris(3-methylimidazol-2-yl)borate) is a C_3-symmetric scorpionate-like, monoanionic *N*-heterocyclic carbene (NHC) donor,[9] which also displayed an S = 1 ground state.[10] Structurally, both the tris(pyrazolyl)borate- and related NHC-ligated complexes display distorted O$_h$ geometries with D$_{3d}$ symmetry (Figure 1).

As previously noted, the X-ray diffraction structures of the [Tp$_2$Mn]$^+$ (**1**) and [Tp*$_2$Mn]$^+$ (**2**) complexes show little distortion from idealized O$_h$ geometry,[11] with each complex having an inversion center and near perfect C_3 axes coincident with the B–Mn–B vector (Figure 1).[2] All N–Mn–N$_{adjacent}$ angles for **1** are within 2.6° of the idealized 90° expected for O$_h$ geometry, and the Mn–N distances fall within the narrow range of 1.979 – 1.988 Å. Complex **2** has slightly longer Mn–N bond lengths (1.992 – 1.999 Å) and N–Mn–N$_{adjacent}$ angles even closer to 90° (89.75 – 90.49°).[2] The solid-state structure of

[{Ph(MeIm)$_3$B}$_2$Mn^{III}]$^+$ (**3**) is similar to those of **1** and **2**, with Mn–C distances ranging from 2.014 – 2.037 Å, but with slightly smaller C–Mn–C$_{adjacent}$ angles of 85.82 – 87.32 Å.[10]

The modest structural changes between **1**, **2**, and **3** nonetheless give rise to differences in axial (*D*) and rhombic (*E*) ground-state zero-field splitting (zfs) parameters. The sign and magnitude of the zfs parameters were determined through high-frequency and -field electron paramagnetic resonance (HFEPR) spectroscopy (**1** and **2**), dc magnetic susceptibility (**1**, **2**, and **3**) and frequency domain Fourier-transform THz-EPR spectroscopy (**1**).[10] Through the HFEPR experiments, the zero field splitting of **1** was characterized as $D = +17.97(1)$, $E = 0.42(2)$ cm^{-1}, and for **2** of $D = +15.89(2)$, $E = 0.04(1)$ cm^{-1}. The dc magnetic susceptibility measurements yielded comparable values, with $D = +18.07$ cm^{-1} for **1** and $D = +14.60$ cm^{-1} for **2**. The facile oxidation of **3** prevented collection of any rational HFEPR data; however, magnetometry measurements for **3** yielded a substantially larger magnitude of *D* than those of **1** and **2**, with an estimate of $D = -49.9$ cm^{-1}. It was suggested that the significantly larger value of *D* for **3** was potentially a sign of an orbitally-degenerate ground state (*i.e.*, ^{3}E), which could result from the much greater σ-donating properties of this ligand. We note for comparison that while zfs parameters were not determined for the previously-reported octahedral $S = 1$ [Mn^{III}(CN)$_6$]$^{3-}$ complex, this species displayed a room-temperature effective magnetic moment significantly above the expected spin-only value ($\mu_{eff} = 3.98$ μ_B versus 2.83 μ_B, respectively), which was attributed to first-order spin-orbit coupling within a ^{3}T$_{1g}$ ground state.[3b] For **1**, **2**, and **3**, density functional theory (DFT) and Hartree-Fock (HF) calculations employed to help understand the ground-state properties of these complexes were able to reproduce the trend in zfs parameters for **1** and **2**, but the *D* values were too low in magnitude by ~40% compared to experiment.[10] Moreover, the DFT approach failed completely when applied to **3**, as a *D* value comparable in magnitude to that of **1** and **2** was predicted (calculated $D = +8.26$ cm^{-1}), in clear disagreement with the experimental estimate.

While the ground-state magnetic properties of **1** and **2** are well-defined, the optical properties are underexplored. All that had been hitherto reported are the diffuse reflectance absorption spectra of **1** and **2** reveal major bands at 390 – 395 and 400 nm, respectively, with shoulders at 460 – 465 and 475 nm.[2,10] The higher-energy features have been attributed to metal-to-ligand charge transfer (MLCT) transitions, while the shoulders are presumed to derive from the ^{3}T$_{1g} \rightarrow {}^3$E$_g$ transition, using symmetry labels from the parent O$_h$ group.[2] Given the rarity of $S = 1$ Mn^{III} centers, further exploration of the optical properties of these complexes is warranted. In addition, better insight into the molecular basis for the significantly enhanced zfs of **3** is also of interest. Overall, understanding how small perturbations in structurally similar complexes give rise to large changes in zfs is an important challenge for contemporary inorganic computational chemistry.[12]

In this work, the electronic structure of **1** and **2** were further explored using low-temperature magnetic circular dichroism (MCD) and variable-temperature, variable-field (VTVH) MCD spectroscopy coupled with *ab initio* complete active space self-consistent field (CASSCF) calculations with second-order *n*-electron valence state perturbation theory (NEVPT2) correction. (We note that corresponding MCD investigations of **3** were repeatedly thwarted by the facile oxidation of this complex, as well as the strong MCD signals of the Mn^{IV}

decay product.) As described elsewhere,[13] analysis of MCD spectra of paramagnetic transition-metal complexes can yield ligand-field and charge-transfer transition energies, which can greatly complement analysis of electronic absorption spectra. Moreover, the VTVH behavior of a given MCD signal is reflective of both ground-state spin Hamiltonian parameters (g-values and, for $S > ½$ systems, zfs parameters) and the transition moment product of the electronic transition under interrogation. Thus, a careful analysis can yield transition polarizations for randomly-oriented samples, which can be a great aid in developing spectral assignments. While this approach has been used with success in analyzing the electronic structure of a limited number of mononuclear Mn^{III} centers in Mn-dependent enzymes[14] and corresponding model complexes,[1e,13e,15] all of these previous examples contained $S = 2$ Mn^{III} centers. To the best of our knowledge, the MCD method has not been applied to Mn^{III} centers with $S = 1$ ground states. Here we have analyzed the variable-temperature behavior of the MCD data of **1** and **2** to provide band assignments that permit a comparison of the electronic structures of these complexes. The results of the MCD analysis are also used to validate the electronic structure computations. The CASSCF/NEVPT2 calculations are able to better reproduce the zfs parameters of **1** and **2** than DFT methods. More significantly, the CASSCF/NEVPT2 calculations properly predict a large magnitude D value for **3**, which can be related to the increased σ-donor properties of the NHC ligands.

RESULTS AND DISCUSSION

Ligand Field Theory Analysis of $S = 1$ Mn^{III} Centers

Before discussing the MCD spectra of **1** and **2**, we first summarize the previously described electronic structure description of these complexes, as this provides an excellent framework for understanding the MCD data. Because of the trigonal symmetry of these complexes, the Mn^{III} $3d$ orbital splitting pattern is atypical for a six-coordinate complex. With the molecular z-axis along the B–Mn–B vector (*i.e.*, the trigonal axis), and thus not oriented along any metal-ligand bond axis, the Mn^{III} $3d_z^2$ orbital (a_{1g} symmetry, using D_{3d} labels) is lowest in energy and doubly-occupied (Figure 2). At higher energy are a set of e_g orbitals ($d_x^2{}_{-y}^2$, d_{xy}), each of which contains one electron. At highest energy, and unoccupied, lie another e_g set (d_{xz}, d_{yz}). It is important to consider that, because of the D_{3d} symmetry there is mixing within and between the e_g sets, and the canonical labels (*i.e.*, $d_x^2{}_{-y}^2$ and d_{xy}) are not meaningful.[16] Although there are alternative frameworks that take such mixing into account,[17] we will nonetheless use the conventional orbital labels for the sake of familiarity.

The ligand-field excited-states arising from this orbital splitting pattern are summarized in Figure 3, where the parent O_h states are included for comparison. The $^3T_{1g}$ ground state of O_h symmetry splits into $^3A_{2g}$ and ^3E_g components. The configurations for these states are shown in Figure 2 (right). On the basis of previous magnetic measurements, **1** and **2** have a $^3A_{2g}$ ground-state, estimated by LFT and AOM calculations to be ~4 000 cm^{-1} below the ^3E_g state.[10] The ground-state of **3** could not be determined from the previous work, although the splitting between the $^3A_{2g}$ and ^3E_g states is certainly smaller. The previous analysis also placed the ^5E_g excited state (i.e., the "conventional", high-spin state) of **1** and **2** at ~14 000 and ~12 000 cm^{-1}, respectively, above the $^3A_{2g}$ ground-state. At significantly

higher energy, there are a cluster of triplet states (Figure 3), all of which should contribute to the optical properties of these complexes.

For **1** and **2**, electronic transition assignments are aided using transition polarizations. For example, $^3A_2 \rightarrow {}^3E$ excitations will be *x,y*-polarized, while $^3A_2 \rightarrow {}^3A_1$ transitions will be *z*-polarized. In principle, transition polarizations can be obtained from analysis of variable-temperature, variable-field MCD data, which are sensitive to both ground-state spin Hamiltonian parameters and transition polarizations.[13b,13c] In this analysis, the MCD signal intensity is monitored as a function of magnetic field strength at various fixed temperatures. Then the resulting MCD curves can be fitted using standard methods. This approach is often used to determine zfs parameters and transition polarizations for paramagnetic metal complexes.[13a–c,13f] However, detailed analysis of VTVH MCD data using common fitting procedures is warranted only when VTVH MCD data collected at a specific wavelength contain contributions from a *single electronic excited state*. The large cluster of closely-space triplet states expected for **1** and **2** (Figure 3) renders this scenario unlikely. Accordingly, we deem it unwise to fit VTVH MCD data for **1** and **2** using standard methods.

However, because **1** and **2** contain triplet ground states with fairly sizeable zero-field splittings, the temperature-dependent behavior of the MCD signals can be used directly to determine transition polarizations. This situation is completely analogous to MCD studies of $S = 1$ $[Fe^{IV}=O]^{2+}$ complexes.[18] As described by Solomon and co-workers,[18c] for such systems, *z*-polarized transitions (i.e., with the external field along *x/y*) will show an inverse temperature dependence that is typical of paramagnetic centers, with signal intensity decreasing as temperature is increased. Under these conditions, the lowest-energy sublevel ($M_S = -1$) is MCD active (Figure 4, right). In contrast, *x,y*-polarized transitions (external field along *z*) will show a more complicated temperature dependence. For these transitions, MCD signal intensity will be small at lowest temperatures, because the MCD-inactive $M_S = 0$ sublevel will be predominantly populated under these conditions (Figure 4, left). MCD intensity for these *x,y*-polarized transitions will show an initial rise with increasing temperature, as the $M_S = -1$ and $+1$ sublevels are thermally populated, and then decrease in intensity at higher temperatures. We note that, unlike the "typical" VTVH MCD analysis, this analysis does not provide quantitative determination of zfs parameters. However, this is not a significant drawback in the present case, as accurate values for the *D* and *E* parameters of **1** and **2** have been determined by other methods.

Magnetic Circular Dichroism Studies of 1 and 2

MCD studies of **1** and **2** were performed to compare the ligand-field transition energies for these complexes, and provide electronic transition energies to use in validating electronic structure computations. MCD data for **2** are discussed first, as their interpretation is marginally more straightforward. MCD spectra collected for **2** at different magnetic field strengths and temperatures are shown in Figure 5 (left and right, respectively). From the variable-field MCD data (Figure 5, left), a minimum of six bands can be identified. Bands 1 and 2 contribute to a pseudo-*A* term (temperature-dependent, derivative-shaped feature), centered at 23 000 cm^{-1}, which dominates the MCD spectra. This MCD features roughly corresponds to the shoulder observed in the solid-state electronic absorption spectrum at 21

100 cm^{-1} that was tentatively assigned as the $^3T_{1g} \rightarrow {}^3E_g$ transition (using O_h symmetry labels).[2] The MCD intensity of the components of the pseudo-A term maximize (*i.e.*, show the most intense positive and negative features) at 15 K, indicating an *x,y*-polarized transition. Thus, the pseudo-A term can be attributed to the $^3A_2 \rightarrow {}^3E$ (^3E_g) excitation (Figure 3), supporting the assignment made for the electronic absorption spectrum of **2**. Indeed, an orbitally-degenerate (or near-degenerate) E excited state should exhibit strong in-state spin-orbit coupling, giving rise to an MCD pseudo-A term.[13a,13b,13d] Bands 3 and 4, which are at slightly higher energy (23 730 and 25 270 cm^{-1}), are *z*-polarized, as the intensity for these bands are maximized at 2 K and decrease with increasing temperature (Figure 5, right). Bands 3 and 4 are therefore assigned as the $^3A_2 \rightarrow {}^3A_1$ ($^3T_{2g}$) and $^3A_2 \rightarrow {}^3A_1$ ($^3A_{1g}$) excitations, respectively.

Bands 5 and 6 form another pseudo-A term centered at 28 800 cm^{-1} (Figure 5). Band 5 appears to show an inverse temperature dependence, consistent with a *z*-polarized transition, although there is no increase in MCD intensity from 8 to 2 K. Band 6 shows a minor increase in intensity with increasing temperature. Thus, band 6 could arise from an *x,y*-polarized transition that is overlapping with *z*-polarized transition(s). In any case, the development of precise band assignments for this spectral region is complicated by the large number of closely-spaced transitions with different MCD signs and temperature dependencies. As described in more detail below, CASSCF/NEVPT2 calculations for **2** predict four electronic transitions from 26 420 – 27 470 cm^{-1}.

At first glance, the MCD spectrum of **1** looks quite different from that of **2** (cf. Figures 5 and 6). Given the structural similarities of these complexes, as well as their similar electronic absorption properties, this is unexpected. However, a more detailed analysis of the temperature- and field-dependence of the MCD spectrum of **1** reveals that its excited-state energies are actually quite similar to those of **2** (Table 1). The major difference is a fairly uniform blue-shift in the transition energies of **1**, which would be consistent with its slightly stronger ligand field, as imposed by shorter Mn–N bond lengths. The difference in appearance of the MCD spectra of **1** and **2** arises because of subtle shifts in the energies of the strongly overlapping *x,y*- and *z*-polarized transitions. For example, band 1 in the MCD spectra of **1** shows an increase in MCD intensity with increasing temperature, with a maximum at 15 K. This behavior marks band 1 as an *x,y*-polarized transition arising from the $^3A_2 \rightarrow {}^3E$ (^3E_g) excitation. The energy of this excitation is blue-shifted, but by only ~900 cm^{-1}, compared to **2**. For **1**, however, the negative component of this pseudo-A term (band 2, 24 500 cm^{-1}) is obscured by overlap with band 3, which is only slightly higher in energy (25 050 cm^{-1}) and shows an inverse temperature dependence characteristic of a *z*-polarized transition. Band 3 is thus assigned as the $^3A_2 \rightarrow {}^3A_1$ ($^3T_{2g}$) excitation, which is blue-shifted by 1 300 cm^{-1} compared to **2** (Table 1). At higher energies, the overlap of several transitions (bands 4 – 6) leads to complex temperature-dependent behavior (Figure 6, right), and unambiguous band assignments are not possible. However, as band 6 shows an increase in MCD intensity from 2 – 8 K, it arises from an *x,y*-polarized transition, and is assigned as the positively-signed component of the $^3A_2 \rightarrow {}^3E$ ($^3T_{2g}$) transition. We tentatively identify the negative-component of this transition to band 4, which occurs near 26 000 cm^{-1} (Figure 6). The temperature-dependence of the MCD signal between 25 500 and

28 000 cm^{-1} requires a negatively-signed MCD signal that maximizes intensity at a temperature other than 2 K (band 4) and a positively-signed MCD signal near 26 000 cm^{-1} with maximum intensity at 2 K (band 5). On the basis of these observations, we attribute band 5 to the $^3A_2 \rightarrow {}^3A_1$ ($^3A_{1g}$) transition. Lastly, band 7, which shows intensity changes as a function of field but not temperature, is tentatively attributed to an MCD *B*-term signal.[13d]

CASSCF/NEVPT2-calculated Electronic Structure

Ligand-field Excited-state Energies for 1 and 2: In order to better understand the MCD properties of **1** and **2**, as well as identify structural and electronic factors contributing to the different zfs of **1, 2**, and **3**,[10] we performed CASSCF/NEVPT2 calculations for these three complexes. This efficient *ab initio* method has been shown to be quite reliable at treating the ground- and excited-state properties of large transition metal complexes.[1e,12,19] First, we will compare the calculated ligand-field excited-state energies with the MCD data of **1** and **2**. Then we will discuss calculated zfs parameters for **1, 2**, and **3** in light of previously published HFEPR and magnetic susceptibility measurements.

Ligand-field state energies from CASSCF/NEVPT2 calculations for **1** and **2** are provided in Table 2 and Figure 7. For both complexes, these calculations predict a $^3A_2$ ground state with a low-lying $^3E(^3T_{1g})$ state at 4 200 and 4 400 cm^{-1}, respectively (because of slight deviations from true D_{3d} symmetry in the models, all ^3E states are split slightly, as shown in Table 2; when referring to E states in the text, we will give the energy of the lowest component). This result is in excellent agreement with previous AOM and LFT calculations for these complexes.[10] The $^5E(^5E_g)$ excited state, which is the lowest-energy quintet state, is at similar energy (4 400 and 3 800 cm^{-1} for **1** and **2**, respectively). Thus, for **2**, $^5E(^5E_g)$ is the lowest-lying excited state. The next triplet excited states for **1** and **2**, $^3E(^3E_g)$, are at 24 250 and 23 140 cm^{-1}, respectively. These calculated energies are not only in excellent agreement with the experimental energies (23 640 and 22 790 cm^{-1}, respectively), the slight red-shift calculated for **2** nicely reproduces the observed trends from the MCD data, where the lowest-energy band of **2** (band 1) is 1 050 cm^{-1} less than the corresponding band of complex **1** (Table 2). For **1**, a cluster of four additional triplet excited states ($^3A_1$, ^3E, $^3A_1$, and $^3A_2$) are predicted within the narrow range of 25 180 and 27 880 cm^{-1} (Table 2), in good agreement with our assignments of bands 3 – 6, which appear from 25 000 to 29 000 cm^{-1} in the MCD spectra of **1** (Figure 6). The corresponding calculated excited states for **2** are red-shifted relative to **1**, appearing from 24 350 to 27 280 cm^{-1} (Table 1), also in excellent agreement with the MCD data for **2** that show a cluster of at least three bands in this region (Figure 5). On the basis of these calculations, band 5 of **2** is tentatively attributed to a component of the $^3A_2 \rightarrow {}^3E(^3T_2)$ excited state. The MCD intensity of this transition should overlap considerably with the MCD intensities of the $^3A_2 \rightarrow {}^3A_1(^3T_2)$ and $^3A_2 \rightarrow {}^3A_1(^3A_1)$ transitions, which are all of similar energy (Table 2). This would account for the unusual temperature dependence of band 5. At slightly higher energy, $^5A_1$ and ^5E excited states are predicted for both complexes. It is possible that these states, as well as charge-transfer excited states, could also contribute to bands 6 and/ or 7 in the higher-energy region of the MCD spectra of **1** and **2**. Taken together, the CASSCF/NEVPT2 excited-state energies corroborate assignments that the visible electronic absorption and MCD features of **1** and **2**

arise from a cluster of closely-spaced triplet excited states. These calculations also reproduce the slightly smaller ligand-field strength imposed by the Tp*⁻ ligands of **2**.

Ground-state zfs Parameters for 1, 2, and 3: The *ab initio* CASSCF/NEVPT2 calculations were also used to provide insight into the zfs parameters of the low-spin Mn^{III} complexes. The D values predicted for **1** and **2** (+16.30 and +14.33 cm⁻¹, respectively; Table 3), are each within 10% (< 2 cm⁻¹ in absolute terms) of their experimental values (+17.97 and +15.89 cm⁻¹, respectively). This is significantly better agreement than that observed for the previously reported DFT-calculated zfs parameters,[10] which are included in Table 3 for comparison. It is important to note that the D value computed by the CASSCF/NEVPT2 method includes only the spin-orbit coupling contribution (D_{SOC}). The spin-spin coupling contribution (D_{SSC}) is omitted. However, the previously-reported CP-DFT computations gave D_{SSC} of 1.0 – 1.8 cm⁻¹,[10] showing that this term is only a minor contributor to the overall D value. The CASSCF/NEVPT2-calculated E/D values are also in good agreement with their experimental counterparts (Table 3), but with **2** predicted to be slightly too rhombic. CASSCF/NEVPT2 calculations for **3** predict a D value of +37.11 cm⁻¹, which is more than twice as large as that of **1** or **2**. This is consistent with the experimental observation that **3** has a D value unusually large in magnitude.[10] However, the calculated D value for **3** is positive, which is in disagreement with the experimental estimate ($D = -49.9$ cm⁻¹). The E/D value calculated for **3** (0.042) is, however, in excellent agreement with the experimental value (0.040).

It must be noted, however, that the experimental situation regarding HFEPR and magnetometry for **3** was much inferior to that for **1** and **2**.[10] Both **1** and **2** have orbitally non-degenerate ground states, well separated in energy from excited states, so that an $S = 1$ spin Hamiltonian analysis of the HFEPR and magnetic data was appropriate and highly successful in fitting both types of measurement with essentially the same parameter set.[10] In contrast, as discussed below, **3** has an electronic ground state that is not as suitable for a simple, spin Hamiltonian analysis. Moreover, complex **3** exhibited no HFEPR spectra and obtaining magnetic data was complicated by the reactivity of the complex. The situation for **3** can be contrasted to that for another, reactive, early transition metal complex with an $S = 1$ ground state, namely *trans*-[TiCl₂(py)₄] (py = pyridine), which contains Ti^{II} (3d²), and has a ³E electronic ground state.[19j] This Ti^{II} complex did exhibit HFEPR spectra, which, together with the magnetic data, were analyzed using an $S = 1$ spin Hamiltonian to yield a large magnitude, but negative D value, with a small rhombic component, which component was the origin of the observed HFEPR signal. The observation of HFEPR for the Ti^{II} complex with its negative D value versus the lack of any HFEPR signal for **3** is consistent with its D value being large in magnitude, but positive in sign, as suggested here by computations.[20] On the other hand, although the determination of sign of zfs solely from magnetic susceptibility is in general problematic,[21] fitting of the experimental dc susceptibility data for **3** was unequivocal in support of a negative value for D (see Figure S1, Supporting Information).

Regardless of the ambiguity in the sign of zfs in **3**, the CASSCF/NEVPT2 calculations also afford the opportunity to understand the basis for the different zfs parameters of **1, 2**, and **3**

in terms of contributions from ligand-field excited states, as shown in Figure 8 and Tables S6 – S8 (Supporting Information). For **1** and **2**, the components of the $^3T_{1g}$ parent state of O_h symmetry make contributions to D of ~2 cm^{-1} in magnitude, but these contributions are of opposite sign and effectively cancel. The dominant contributions to D come from singlet excited states; in particular the $^1A_1(^1T_{2g})$ and $^1A_1(^1A_{1g})$ excited states both provide large positive contributions (Figure 8). For **1**, these excited states are at slightly lower energy and make larger contributions, accounting for the increase in magnitude of D for **1** as compared with **2**. For complex **3**, the $^1A(^1T_{2g})$ and $^1A_1(^1A_{1g})$ states still make large contributions to D, but the low-lying $^3E(^3T_{1g})$ state makes the dominant contribution. The $^3E(^3T_{1g})$ state of **3** is only ~1 000 cm^{-1} higher in energy than the $^3A_2$ ground state, which would lead to stronger mixing between these states. Thus, the large increase in D of **3** compared to **1** and **2** has its origin in a substantially smaller splitting between the $^3A_2$ ground state and lowest $^3E(^3T_{1g})$ excited state.

For all three complexes, contributions to the rhombic zfs parameter E come predominantly from components of the parent $^3T_{1g}$ ground state, and, in the case of **1** and **2**, the $^1E(^1T_{1g})$, states also contribute (Figure 8, right). However, the different components of these E states make oppositely-signed contributions to E. Because these E excited states are nearly degenerate, their oppositely-signed contributions are roughly equal in magnitude, which accounts for the small E values observed for each complex. On the basis of these observations, the slightly larger rhombicity of **3** can be attributed to larger, albeit still quite small, distortions from true trigonal symmetry.

Electronic Structures Descriptions of 1, 2, and 3: As described above, changes in the ligand-field excited-state energies of **3**, compared to **1** and **2**, can account for large changes observed in zfs parameters. In this section we discuss the structural and electronic differences that account for these observations. On the basis of the CASSCF/NEVPT2 calculations, **1** and **2** contain $^3A_2$ ground states, arising from a $(d_{z^2})^2(d_{xy}, d_{x^2-y^2})^2(d_{xz}, d_{yz})^0$ configuration (95% contribution to the CASSCF wavefunction). For each of these complexes, the higher-energy $(d_{z^2})^1(d_{xy}, d_{x^2-y^2})^3(d_{xz}, d_{yz})^0$ configuration makes only a 1% contribution to the ground-state wavefunction. Figure 9 shows surface contour plots of the CASSCF frontier orbitals for **1**; corresponding plots for **2** and **3** are in Supporting Information (Figures S2 and S3). These orbital plots echo the bonding description anticipated from ligand-field theory (Figure 1); they also highlight the high degree of mixing between the e(d_{xy}, $d_{x^2-y^2}$) and e(d_{xz}, d_{yz}) sets.

Although the CASSCF/NEVPT2 calculations show that **3** retains a $^3A_2$ ground state, the lowest-lying ^3E excited state is now only ~1 000 cm^{-1} higher in energy. In addition, the ground-state CASSCF wavefunction for **3** contains modest multiconfigurational character, being composed of 87% $(d_{z^2})^2(d_{xy}, d_{x^2-y^2})^2(d_{xz}, d_{yz})^0$ and 11% $(d_{z^2})^1(d_{xy}, d_{x^2-y^2})^3(d_{xz}, d_{yz})^0$. Another marked difference for **3** is that the higher-energy triplet excited states are blue-shifted dramatically, as seen in Figure 7. In fact, after the $^3E(^3T_{2g})$ state, the lowest-energy triplet excited state is at 33 550 cm^{-1}. This result appears to be in conflict with the electronic absorption spectrum of **3**, which shows bands at ~550 and 400 nm (18 180 and 25 000 cm^{-1}). Accordingly, the high energy of the calculated excited states is very likely an

artifact of the CASSCF/NEVPT2 calculations. A common drawback of the CASSCF method is that it leads to an overly ionic description of bonding. While the purpose of the NEVPT2 correction is to remedy this deficiency through the introduction of dynamic correlation, the extent to which this occurs can vary from system to system.[19g] Unfortunately, our attempts to compensate through a larger CAS(8,7) active space met with failure due to lack of CASSCF convergence even when using modest level shifting.

The small splitting between the $^3A_2$ and ^3E states of **3** can be understood on the basis of the increased σ-donation of the NHC ligand. The strong σ-donating ability of this type of NHC ligand was previously identified for a set of four-coordinate Ni^{II} complexes through classical LFT.[22] To illustrate the difference in covalency among these three Mn^{III} complexes, we turned to ground-state DFT computations. As shown in Table 4, the Mn^{III} $3d_z{}^2$ MO of **3** is more covalent than those of **1** and **2**, containing three-fold greater ligand character. In addition, the $3d_z{}^2$ MO of **3** is mixed with the $3d_{yz}$ MO, causing its appearance to differ substantially compared to the corresponding MOs for **1** and **2** (Figure 10). This enables π-interactions between the $3d_z{}^2$ orbital of the Mn^{III} center and the NHC ligand, which further destabilizes this MO. The $3d_z{}^2$-$3d_{yz}$ mixing in **3** is presumably related to slightly larger distortions from true D_{3d} symmetry for this complex as compared to **1** and **2**.[10] In contrast, the ligand character in the Mn^{III} $3d_{x^2-y^2}$ and $3d_{xy}$ MOs of all complexes is equal (~50% when summed over both MOs). Consequently, the $3d_z{}^2$–($3d_{x^2-y^2}$, $3d_{xy}$) splitting is smaller for **3** than for **1** and **2** (2.7 eV versus 4 eV). This effect is illustrated in Figure 10 and is consistent with the results of the CASSCF/NEVPT2 computations. It could be envisioned that structural differences between **1, 2**, and **3** facilitate greater σ-overlap between the NHC donors and the Mn $3d_z{}^2$ orbital by contracting the C–Mn···B angles and distorting the donor atoms away from the Mn center along the z-axis (the Mn···B vector),. However, the average C–Mn···B angles of **3** (52.5°) are only marginally smaller than the corresponding N–Mn···B angles of **1** and **2** (53.3° and 54.8°, respectively). Thus, any increase in σ-covalency of the Mn^{III} $3d_z{}^2$ MO is predominantly electronic in origin, and relates to the far greater σ-donating properties of the NHC ligand as compared to Tp$^-$ and Tp*$^-$. At the same time, the distortions from true trigonal symmetry for **3** appear to facilitate greater π-covalency in the $3d_z{}^2$ MO, which further decreases the $3d_z{}^2$–($3d_{x^2-y^2}$, $3d_{xy}$) splitting.

Conclusions

Six-coordinate Mn^{III} in the absence of very strong field ligands (e.g., cyanide) typically affords high-spin ($S = 2$) complexes, with some interesting exceptions.[4–5] The remarkable and versatile scorpionate ligand, both in its original, hydridotris(pyrazolyl)borate form, and in a newer aryltris(carbene)borate form, which comprises the popular *N*-heterocyclic carbene (NHC) donor, leads to bis(scorpionate) complexes of Mn^{III} in the low spin (based on octahedral geometry conventions) state ($S = 1$). This phenomenon can be attributed qualitatively to the strong donor properties of the scorpionate ligand in combination with the rigorously trigonal symmetry of the bis(scorpionate) Mn^{III} complexes. However, a deeper understanding of this phenomenon had not been provided as the computational requirements for such an analysis are significant. Additionally, such an analysis requires knowledge of the electronic excited states of the complex, which had not been apparent from electronic

absorption spectroscopy. MCD spectroscopy, however, provides such information quite effectively. This approach has been shown to be quite powerful in the treatment of high-spin Mn^{III} centers.[1e,13e,14a,14c–f,15a,15b] As demonstrated here, MCD spectroscopy is equally adept at treating low-spin Mn^{III} systems. This technique, particularly with the use of variable fields and temperatures (VTVH-MCD) allowed elucidation of the range of relevant electronic excited states for **1** and **2**. Unfortunately, the propensity of **3** to oxidize to its Mn^{IV} congener, which complex (in the characterized form, $[\{PhB(MeIm)_3\}_2Mn](CF_3SO_3)_2)$, is itself of interest and exhibits very strong absorption bands, precluded MCD studies of **3**. This is unfortunate, as such studies would have not only provided electronic transition energies, but could also have helped determine the sign of D. At present, the D value of -49.90 cm^{-1} for **3** rests on fits of previously reported dc magnetic susceptibility measurements.[10] All attempts to refine this value, through HF-EPR or MCD measurements, have been hampered by the instability of **3** towards oxidation to the Mn^{IV} form. Nevertheless, computational studies of **3** demonstrated a significant difference from **1** and **2**, namely that the lowest lying triplet excited state is much closer in energy in the tris(carbene)borate complex, a consequence of the strong σ-donor properties of the NHC ligand. This was previously postulated on the basis of a detailed ligand-field theory analysis of these complexes.[10] In general, the previous ligand-field theory analysis is fully consistent with the results of the CASSCF/NEVPT2 computations, illustrating the power of this traditional approach. The higher-energy Mn^{III} d_z^2 MO in **3**, as established by the computations described here, might be the basis for **3** being remarkably easy to oxidize, with the Mn^{IV} oxidation state stabilized by over 1 V in comparison to **1** and **2**.[23] In any case, this difference in electronic structure is indeed the basis for the much larger magnitude zfs in **3** versus **1** and **2**, which led to the previously observed dramatic differences in magnetic susceptibility and HFEPR spectroscopic behavior for the two types of complexes, and suggesting a role for supporting ligands in tuning zfs. Our combined VTVH-MCD and initio computational methods have unraveled the electronic structure of a series of unusual bis(scorpionate) complexes of Mn^{III}, revealing the impact of the great tunability of the scorpionate ligand.

EXPERIMENTAL AND THEORETICAL METHODS

Materials

Solid samples of **1** and **2** with SbF_6^- as the counteranion were either supplied by F. A. Schultz or prepared following the procedure his group reported.[2] A solid sample of **3** with $CF_3SO_3^-$ as the counteranion was prepared as previously described.[10] All other chemicals were obtained from commercials vendors and used without further purification.

Magnetic Circular Dichroism Experiments

Magnetic circular dichroism (MCD) spectra were collected on a spectropolarimeter (Jasco J-815) interfaced with a magnetocryostat (Oxford Instruments SM-4000-8) capable of horizontal fields up to 8 T. MCD spectra were collected at 2, 4, 8, and 15 K for positive and negative field strengths of 1 to 7 T in 1 T increments. All MCD samples were prepared as thin mull samples by preparing a thick paste using Fluorolube®. Unfortunately, although prepared in an argon-filled glovebox and immediately flash-frozen in liquid nitrogen upon

removal from the box, we were unable to collect MCD spectra for **3** that were not contaminated with signals associated with the Mn^{IV} oxidation product, $[\{PhB(MeIm)_3\}_2Mn^{IV}]^{2+}$, which has been previously reported as the bis(triflate) salt,[23] prepared via oxidation of a Mn^{I} precursor, rather than from **3**. The MCD properties of $[\{PhB(MeIm)_3\}_2Mn^{IV}]^{2+}$ are of interest in their own right and will be reported in a separate study.

Computational Methods

The ORCA 3.0.1 software package[24] was used for DFT and *ab initio* CASSCF/NEVPT2 calculations. Initial models of **1, 2**, and **3** were obtained from X-ray crystal structures,[2,10] and used for subsequent calculations without modification. In the case of **1** and **3**, subsequent calculations were also performed using models where the positions of the hydrogen atoms were energy minimized using DFT methods, but all other atoms retained their crystallographic positions. Comparison of calculated zfs parameters for these two structures revealed only very minor changes (changes in D of less than 0.2 cm^{-1}) following the constrained optimization. Cartesian coordinates for all complexes examined are included in Supporting Information (Tables S1 – S5). DFT calculations[25] performed for **1, 2**, and **3** used the B3LYP functional[26] and SVP (Ahlrichs split valance polarized)[27] basis set with the SV/J auxiliary basis set on carbon and hydrogen atoms with the larger TZVP (Ahlrichs triple-ζ valence polarized) on manganese, nitrogen, and boron atoms (for **1** and **2**) as well as the coordinating carbon atoms (for **3**). The resolution of identity (RIJCOSX)[28] approximation was used for all calculations. State-averaged CASSCF/NEVPT2 calculations[29] employed the RI approximation and the SVP basis set for carbon and hydrogen as well as the TZVP basis set for manganese, nitrogen, boron, and coordinating C (for **3**) atoms. For **1, 2**, and **3**, the calculations were performed with five quintet roots, ten triplet roots, and ten singlet roots and the active space CAS(4,5). A representative ORCA input file for the CASSCF/NEVPT2 calculation of **1** is given in Supporting Information.

Supplementary Material

Refer to Web version on PubMed Central for supplementary material.

Acknowledgments

References

1. a) Kitajima N, Komatsuzaki H, Hikichi S, Osawa M, Moro-oka Y. J. Am. Chem. Soc. 1994; 116:11596–11597.b) Kitajima N, Osawa M, Tanaka M, Morooka Y. J. Am. Chem. Soc. 1991; 113:8952–8953.c) Osawa M, Fujisawa K, Kitajima N, Moro-oka Y. Chem. Lett. 1997; 26:919–920.d) Singh UP, Sharma AK, Hikichi S, Komatsuzaki H, Moro-oka Y, Akita M. Inorg. Chim. Acta. 2006; 359:4407–4411.e) Colmer HE, Geiger RA, Leto DF, Wijeratne GB, Day VW, Jackson TA. Dalton Trans. 2014; 43:17949–17963. [PubMed: 25312785]

2. Hossain F, Rigsby MA, Duncan CT, Milligan PL, Lord RL, Baik MH, Schultz FA. Inorg. Chem. 2007; 46:2596–2603. [PubMed: 17330969]

3. a) Blake AB, Figgis BN, Reynolds PA, Engelhardt LM, Moubaraki B, Murray KS. J. Chem. Soc., Dalton Trans. 1994:1121–1123.b) Buschmann WE, Liable-Sands L, Rheingold AL, Miller JS. Inorg. Chim. Acta. 1999; 284:175–179.

4. Ganguly S, Karmakar S, Chakravorty A. Inorg. Chem. 1997; 36:116–118.

5. Basu P, Chakravorty A. Inorg. Chem. 1992; 31:4980–4986.

6. Hansen AP, Goff HM. Inorg. Chem. 1984; 23:4519–4525.

7. Landrum JT, Hatano K, Scheidt WR, Reed CA. J. Am. Chem. Soc. 1980; 102:6729–6735.

8. Mossin S, Sorensen HO, Weihe H. Acta Crystallogr C. 2002; 58:M204–M206. [PubMed: 11932516]

9. Smith JM. Comments on Inorganic Chemistry. 2008; 29:189–233.

10. Forshaw AP, Smith JM, Ozarowski A, Krzystek J, Smirnov D, Zvyagin SA, Harris TD, Karunadasa HI, Zadrozny JM, Schnegg A, Holldack K, Jackson TA, Alamiri A, Barnes DM, Telser J. Inorg. Chem. 2013; 52:144–159. [PubMed: 23259486]

11. The X-ray structures of **1** and **2** were of the SbF$_6$$^-$ salts-**1**(SbF$_6$), and **2**(SbF$_6$), which we have also examined here. The related X-ray structure of **3** was of the triflate (OTf$^-$ = CF$_3$SO$_3$ $^-$) salt, **3**(OTf).

12. Atanasov M, Aravena D, Suturina E, Bill E, Maganas D, Neese F. Coord. Chem. Rev. 2015; 289–290:177–214.

13. a) Kirk ML, Peariso K. Curr. Opin. Chem. Biol. 2003; 7:220–227. [PubMed: 12714055] b) Neese F, Solomon EI. Inorg. Chem. 1999; 38:1847–1865. [PubMed: 11670957] c) Oganesyan VS, George SJ, Cheesman MR, Thomson AJ. J. Chem. Phys. 1999; 110:762–777.d) Piepho, SB., Schatz, PN. Group Theory in Spectroscopy with Applications to Magnetic Circular Dichroism. New York: Wiley; 1983. p. 634e) Westphal A, Klinkebiel A, Berends H-M, Broda H, Kurz P, Tuczek F. Inorg. Chem. 2013; 52:2372–2387. [PubMed: 23410227] f) Paulat F, Lehnert N. Inorg. Chem. 2008; 47:4963–4976. [PubMed: 18438984]

14. a) Whittaker J, Whittaker M. J. Am. Chem. Soc. 1991; 113:5528–5540.b) Jackson TA, Brunold TC. Acc. Chem. Res. 2004; 37:461–470. [PubMed: 15260508] c) Jackson TA, Gutman CT, Maliekal J, Miller A-F, Brunold TC. Inorg. Chem. 2013; 52:3356–3367. [PubMed: 23461587] d) Jackson TA, Karapetian A, Miller A-F, Brunold TC. J. Am. Chem. Soc. 2004; 126:12477–12491. [PubMed: 15453782] e) Jackson TA, Xie J, Yikilmaz E, Miller A-F, Brunold TC. J. Am. Chem. Soc. 2002; 124:10833–10845. [PubMed: 12207539] f) Jackson TA, Yikilmaz E, Miller A-F, Brunold TC. J. Am. Chem. Soc. 2003; 125:8348–8363. [PubMed: 12837107]

15. a) Geiger RA, Wijeratne G, Day VW, Jackson TA. Eur. J. Inorg. Chem. 2012:1598–1608.b) Geiger RA, Chattopadhyay S, Day VW, Jackson TA. J. Am. Chem. Soc. 2010; 132:2821–2831. [PubMed: 20136141] c) Linder RE, Rowlands JR. Spectrosc. Lett. 1971; 4:227–236.

16. This orbital mixing is more extensive than that observed for a system with D_{3h} symmetry, as in that case, the d$_{xy}$ and d$_{x^2-y^2}$ orbitals transform as e$'$, while the d$_{xz}$ and d$_{yz}$ orbitals transform as e$''$

17. a) McGarvey BR. J. Chem. Phys. 1963; 38:388–392.b) McGarvey BR, Telser J. Inorg. Chem. 2012; 51:6000–6010. [PubMed: 22583045]

18. a) Decker A, Rohde J-U, Klinker EJ, Wong SD, Que L Jr. Solomon EI. J. Am. Chem. Soc. 2007; 129:15983–15996. [PubMed: 18052249] b) Decker A, Clay MD, Solomon EI. J. Inorg. Biochem. 2006; 100:697–706. [PubMed: 16510189] c) Decker A, Rohde J-U, Que L Jr. Solomon EI. J. Am. Chem. Soc. 2004; 126:5378–5379. [PubMed: 15113207]

19. a) Duboc C, Ganyushin D, Sivalingam K, Collomb M-N, Neese F. J. Phys. Chem. A. 2010; 114:10750–10758. [PubMed: 20828179] b) Zadrozny JM, Atanasov M, Bryan AM, Lin C-Y, Rekken BD, Power PP, Neese F, Long JR. Chem. Sci. 2013; 4:125–138.c) Atanasov M, Zadrozny JM, Long JR, Neese F. Chem. Sci. 2013; 4:139–156.d) Atanasov M, Ganyushin D, Pantazis DA, Sivalingam K, Neese F. Inorg. Chem. 2011; 50:7460–7477. [PubMed: 21744845] e) Maganas D, Krzystek J, Ferentinos E, Whyte AM, Robertson N, Psycharis V, Terzis A, Neese F, Kyritsis P. Inorg. Chem. 2012; 51:7218–7231. [PubMed: 22697407] f) Atanasov M, Comba P, Helmle S, Müller D, Neese F. Inorg. Chem. 2012; 51:12324–12335. [PubMed: 23102238] g) Schweinfurth D, Sommer MG, Atanasov M, Demeshko S, Hohloch S, Meyer F, Neese F, Sarkar B. J. Am. Chem. Soc. 2015; 137:1993–2005. [PubMed: 25588991] h) Schapiro I, Sivalingam K, Neese F. J.

Chem. Theory Comput. 2013; 9:3567–3580. [PubMed: 26584112] i) Atanasov M, Ganyushin D, Sivalingam K, Neese F. Struct. Bonding (Berlin, Ger.). 2012; 143:149–220.j) Wijeratne GB, Zolnhofer EM, Fortier S, Grant LN, Carroll PJ, Chen C-H, Meyer K, Krzystek J, Ozarowski A, Jackson TA, Mindiola DJ, Telser J. Inorg. Chem. 2015; 54:10380–10397. [PubMed: 26451744]

20. MCD investigations of **3** were complicated by the strong absorption bands of the Mn(IV) decomposition product. HFEPR of **3** did show some Mn(IV), but this Kramers (half-integer spin) signal is narrow and easily identified and would not interfere with signal from the non-Kramers (integer spin) complex **3**. Relaxation effects, which may be significant due to the close lying excited state, may also prevent observation of HFEPR, even in the case of a negative D value.

21. Kahn, O. Molecular Magnetism. New York, NY: VHC Publishers, Inc.; 1993.

22. Nieto I, Bontchev RP, Ozarowski A, Smirnov D, Krzystek J, Telser J, Smith JM. Inorg. Chim. Acta. 2009; 362:4449–4460.

23. Forshaw AP, Bontchev RP, Smith JM. Inorg. Chem. 2007; 46:3792–3794. [PubMed: 17425307]

24. a) Neese, F. ORCA - an ab initio, Density Functional and Semiempirical Program Package, Version 3.0. Max Planck Institute for Chemical Energy Conversion; 2013. b) Neese F. Wiley Interdisciplinary Reviews: Computational Molecular Science. 2012; 2:73–78.

25. Neese F. J. Chem. Phys. 2007; 127:164112–164119. [PubMed: 17979324]

26. a) Becke AD. J. Chem. Phys. 1993; 98:1372–1377.b) Becke AD. J. Chem. Phys. 1993; 98:5648–5652.c) Lee C, Yang W, Parr RG. Phys. Rev. B. 1988; 37:785–789.

27. a) Schäfer A, Horn H, Ahlrichs R. J. Chem. Phys. 1992; 97:2571–2577.b) Schäfer A, Huber C, Ahlrichs R. J. Chem. Phys. 1994; 100:5829–5835.

28. Neese F. J. Comput. Chem. 2003; 24:1740–1747. [PubMed: 12964192]

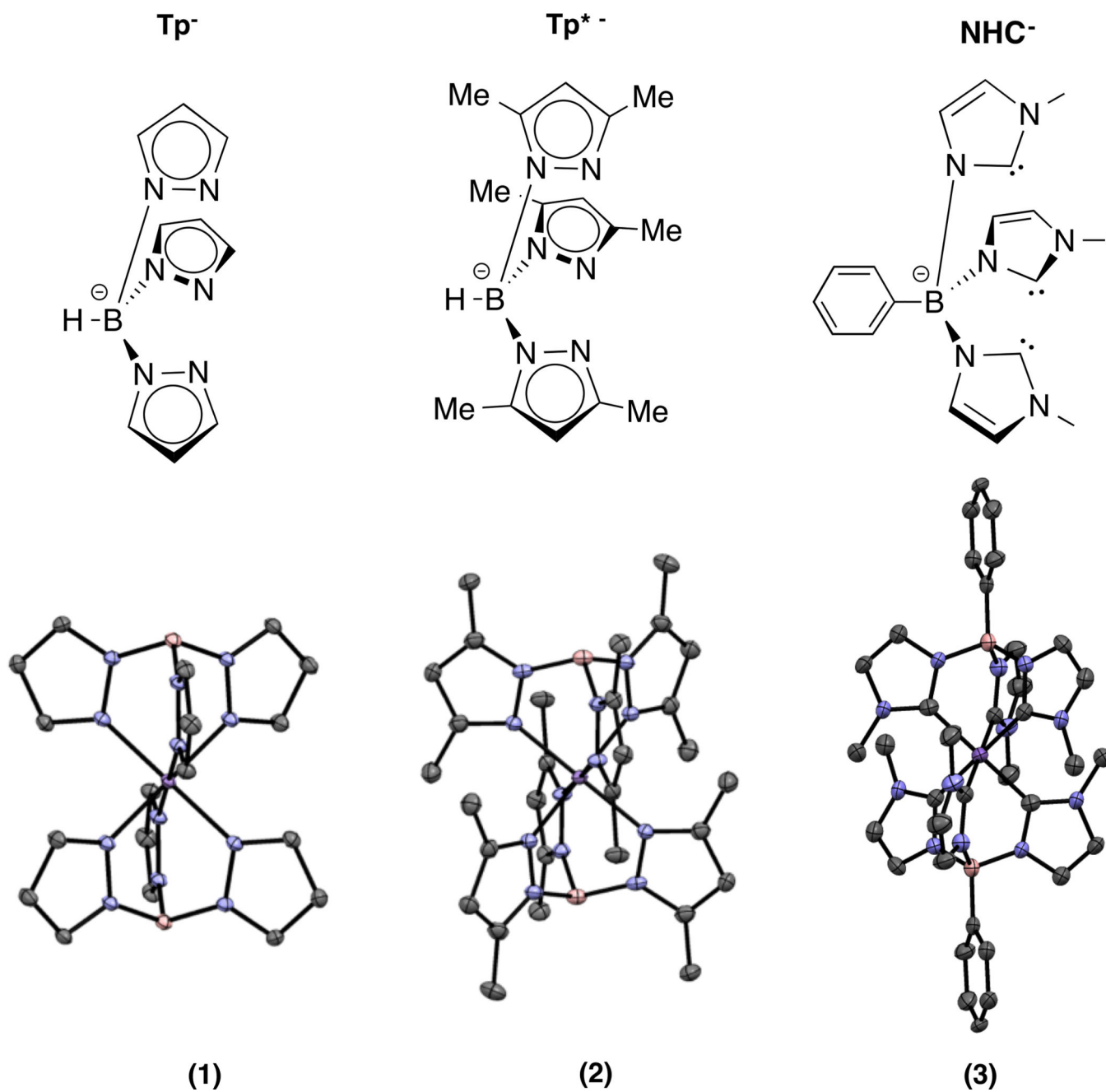29. Angeli C, Cimiraglia R, Evangelisti S, Leininger T, Malrieu J-P. J. Chem. Phys. 2001; 114:10252–10264.

Tp⁻

Tp* ⁻

NHC⁻

(1)

(2)

(3)

Figure 1.
Tp⁻, Tp*⁻, and PhB(MeIm)₃⁻(NHC⁻) ligands (top) and XRD structures[2,10] of **1**, **2**, and **3** (bottom).
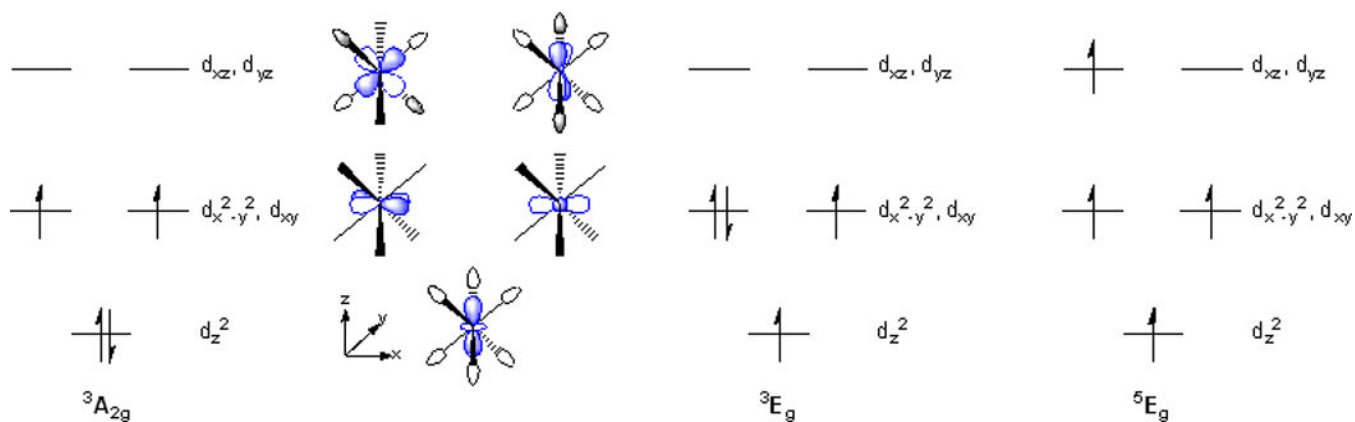
Figure 2.
Left: Low-spin d^4 orbital splitting of **1, 2**, and **3** in D_{3d} symmetry with ground state electron occupancy and schematic MO plots showing Mn^{III} $3d$ orbitals with appropriate symmetry-adapted linear combinations of ligand orbitals. Right: Electron occupancies for the two lowest excited states, ^3E_g and ^5E_g, are shown for comparison.
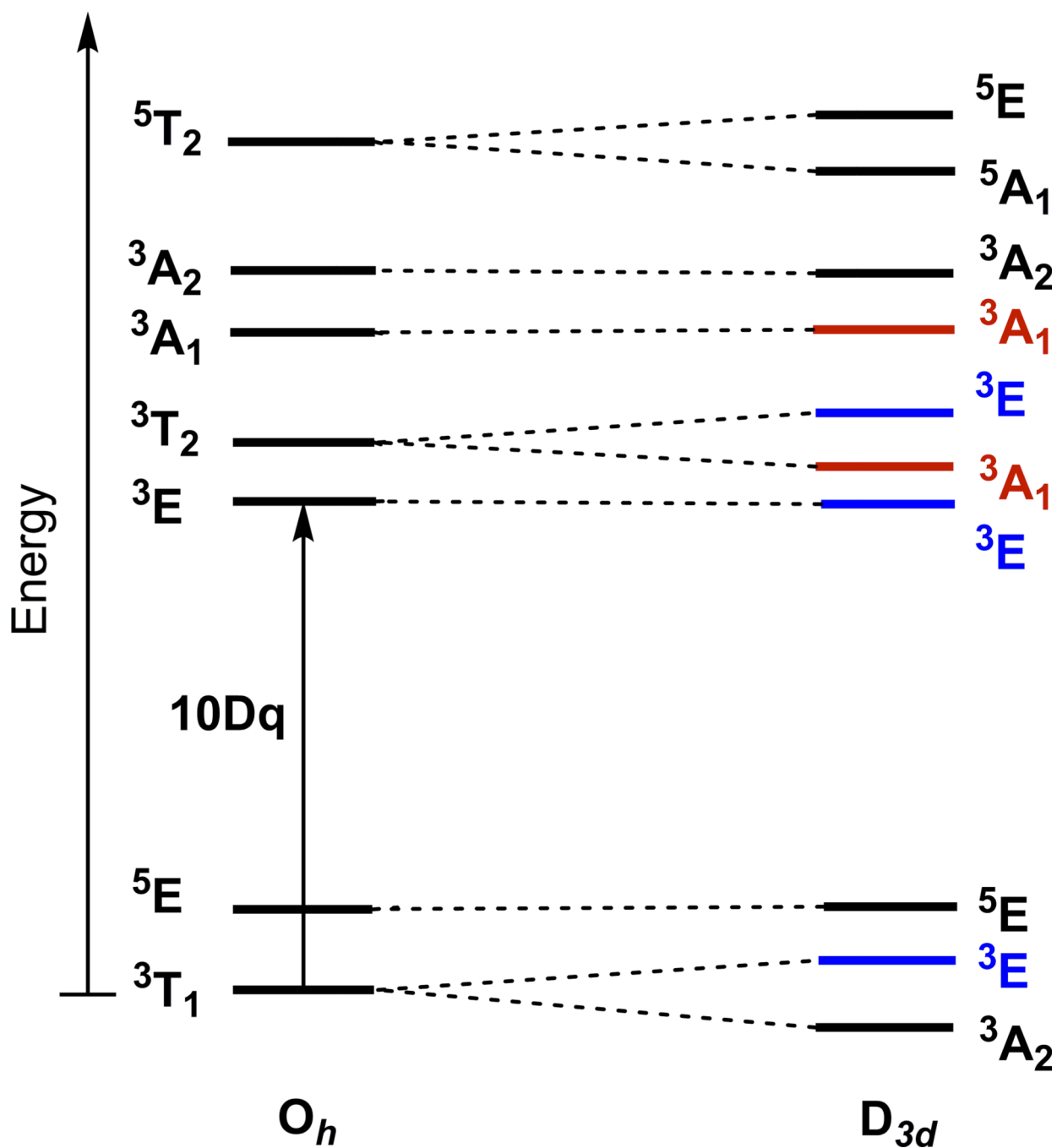
Figure 3.
Ligand-field energy level diagram for $S = 1$ Mn^{III} (d^4) system in O_h and D_{3d} symmetries (g subscripts have been omitted for clarity in both cases). The ^3E (blue) and $^1A_1$ (red) excited states will give rise to x,y- and z-polarized transitions, respectively.
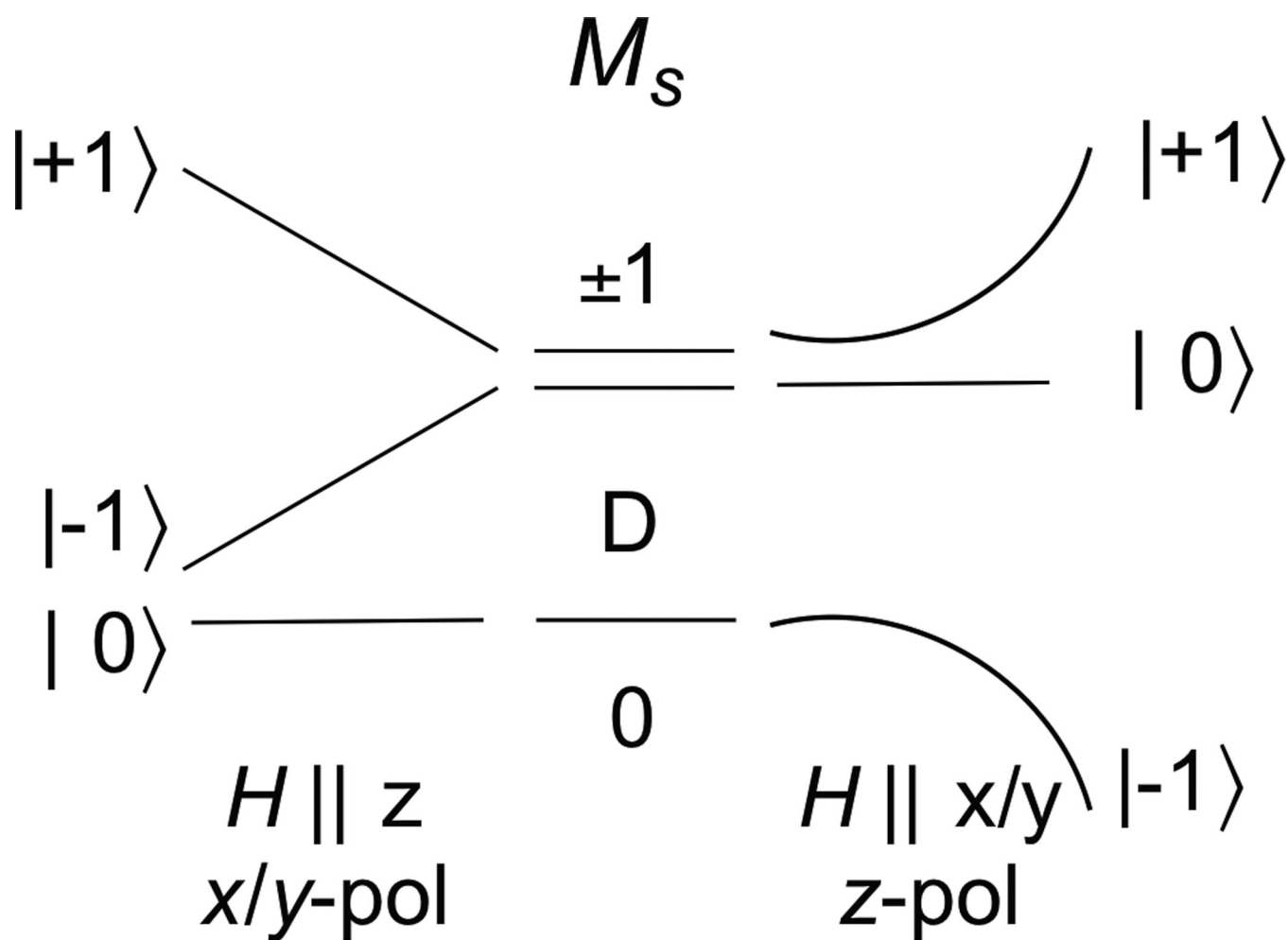
Figure 4.
Magnetic-field-induced splitting of M_s sublevels for an $S = 1$ ground state with sizeable zfs (D). The left-hand side shows the response of an $S = 1$ ground state when the magnetic field is along the z-axis, which would correspond to an x,y-polarized transition. The right-hand side shows the response when the magnetic field is along the x/y-axis, which would correspond to a z-polarized transition. This analysis assumes a small rhombic splitting, which is appropriate for **1** and **2**.
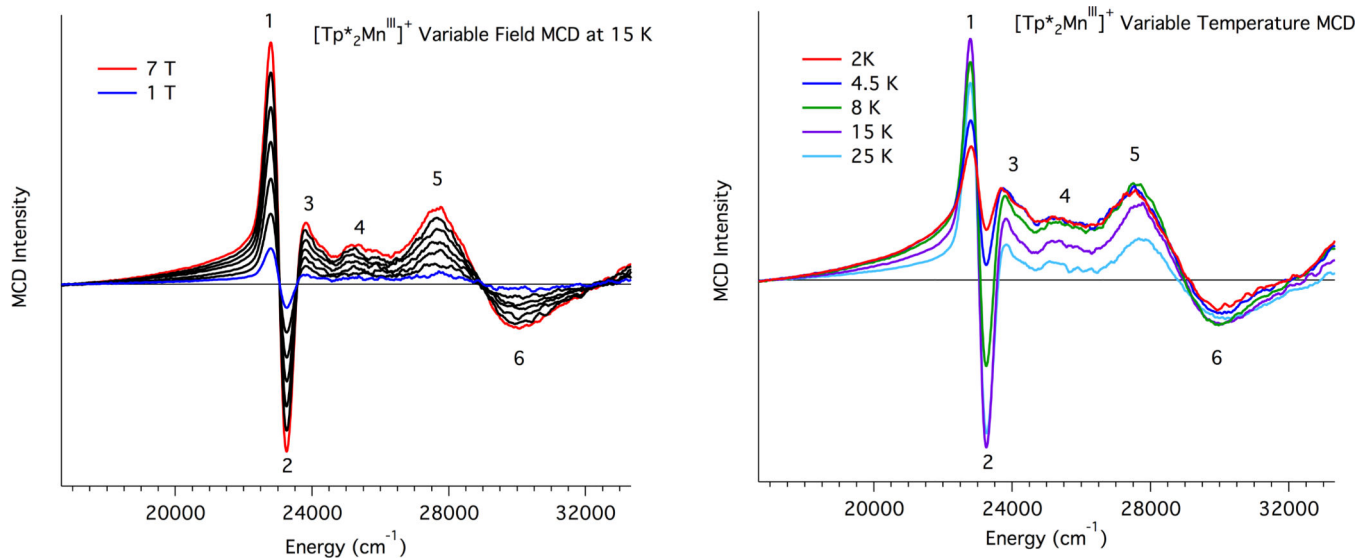
Figure 5.
15 K variable-field (left; field decreasing from 7 to 1 T in 1 T increments; the 7 T trace is in red and the 1 T trace is in blue) and 7 T variable-temperature (right) MCD spectra of a mull sample of **2**.

Figure 6.
8 K variable-field (left; field decreasing from 7 to 1 T in 1 T increments; the 7 T trace is in red and the 1 T trace is in blue) and 7 T variable-temperature (right) MCD spectra of a mull sample of **1**.
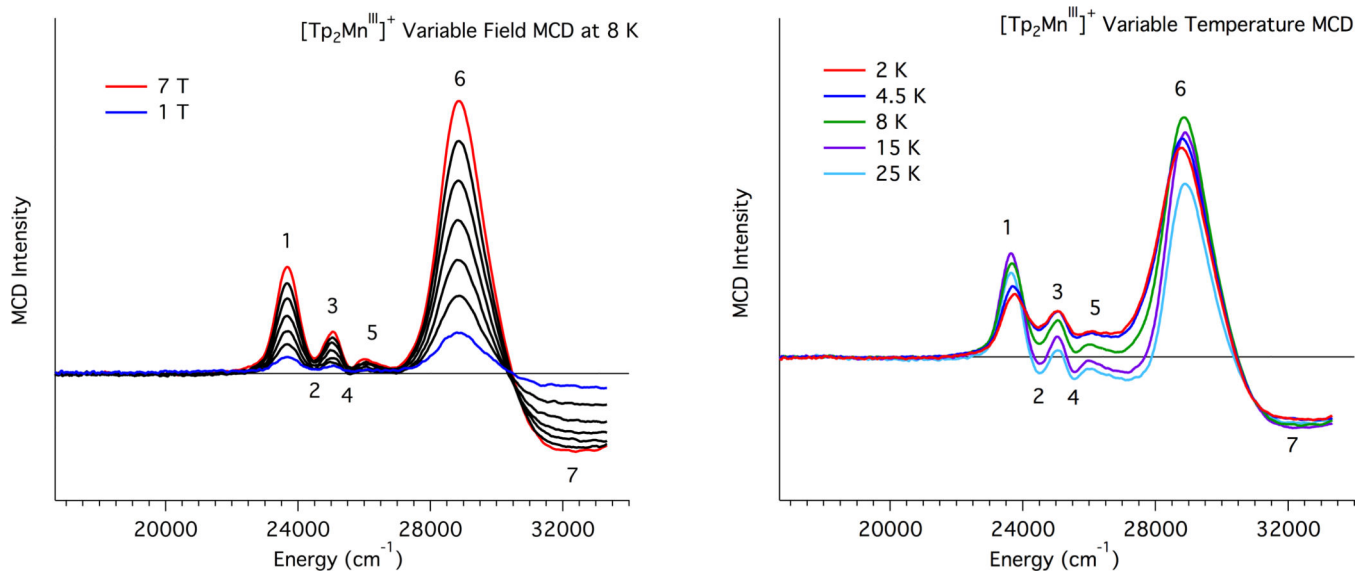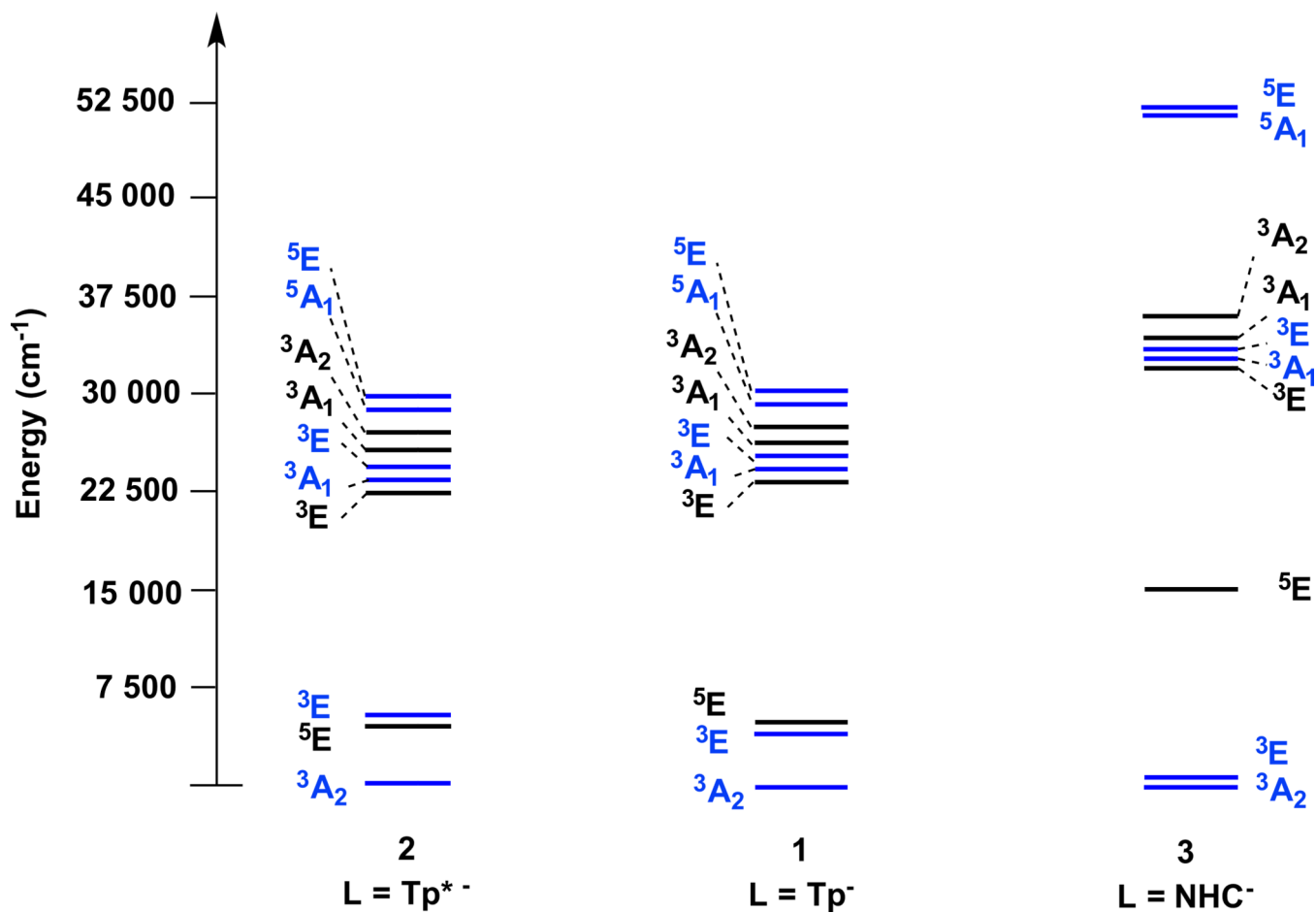
Figure 7.
CASSCF/NEVPT2-calculated states for **2** (left), **1** (center), and **3** (right).
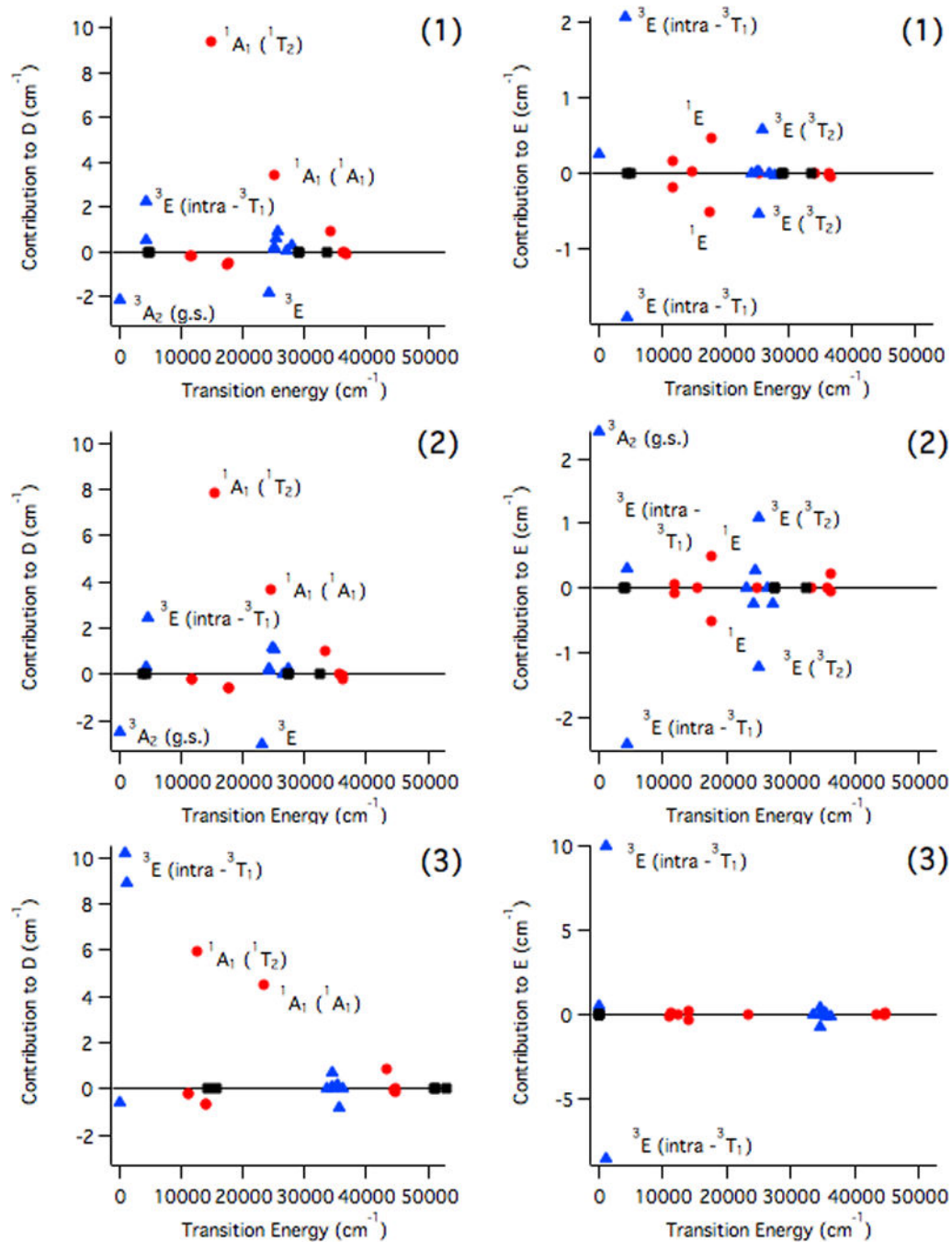
Figure 8.
Contributions of excited state singlets (red circles), triplets (blue triangles), and quintets (black squares) to D (left) and E (right) for **1** (top), **2** (middle), and **3** (bottom).
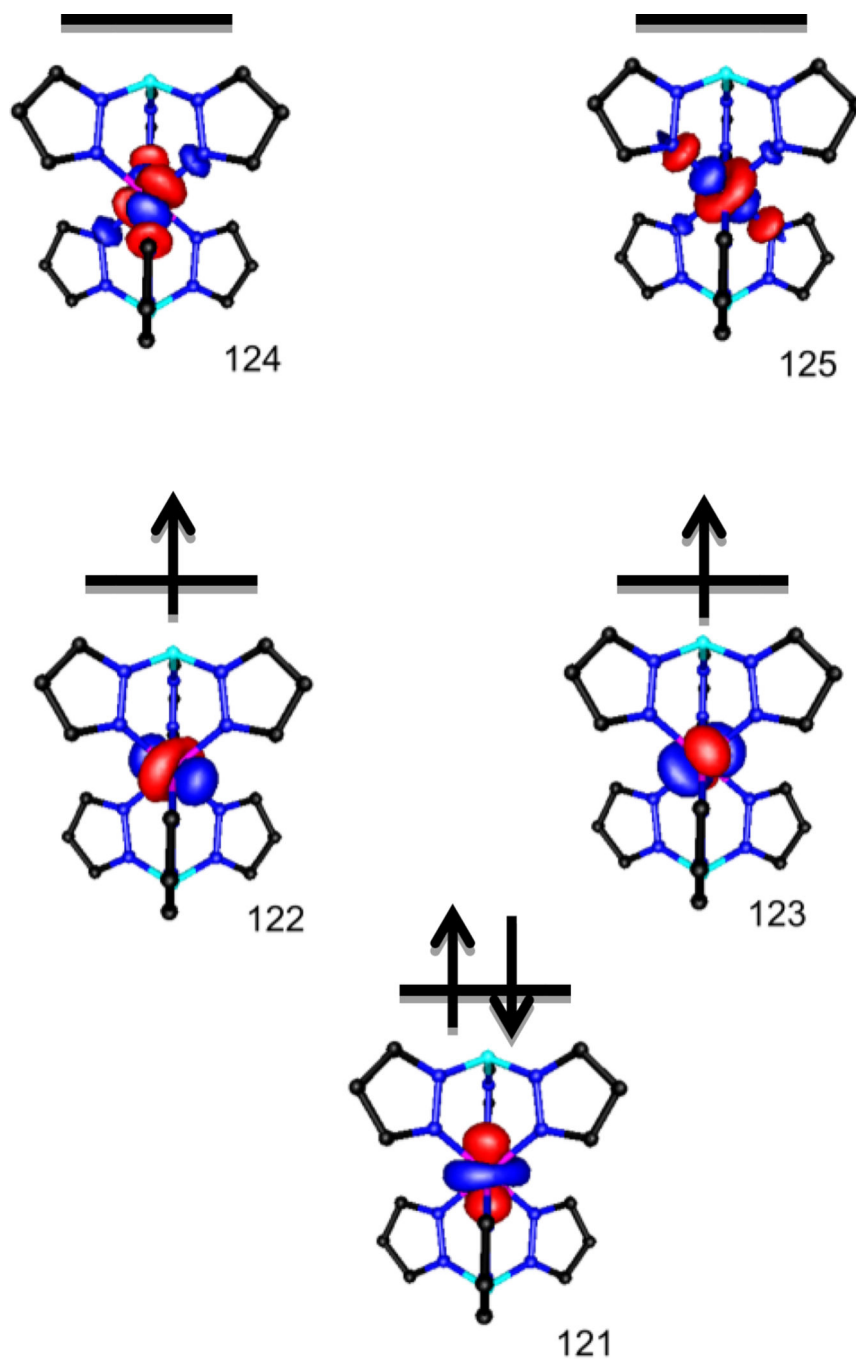
Figure 9.
Surface contour plots of Mn^{III} 3d-based orbitals for **1** from the CASSCF calculation, with the orbital numbers reflecting the energy ordering. Corresponding orbitals for **2** and **3** are shown in Supporting Information (Figures S2 and S3, respectively).

Figure 10.
Energies of Mn^{III} frontier MOs of **1, 2**, and **3**, highlighting the strong destabilization of the d$_z^2$ MO of **3**. Surface contour plots of the Mn^{III} d$_z^2$ MO of each complex are shown.

Table 1

MCD Band Energies,[a] Polarizations, and Assignments for **2** and **1**

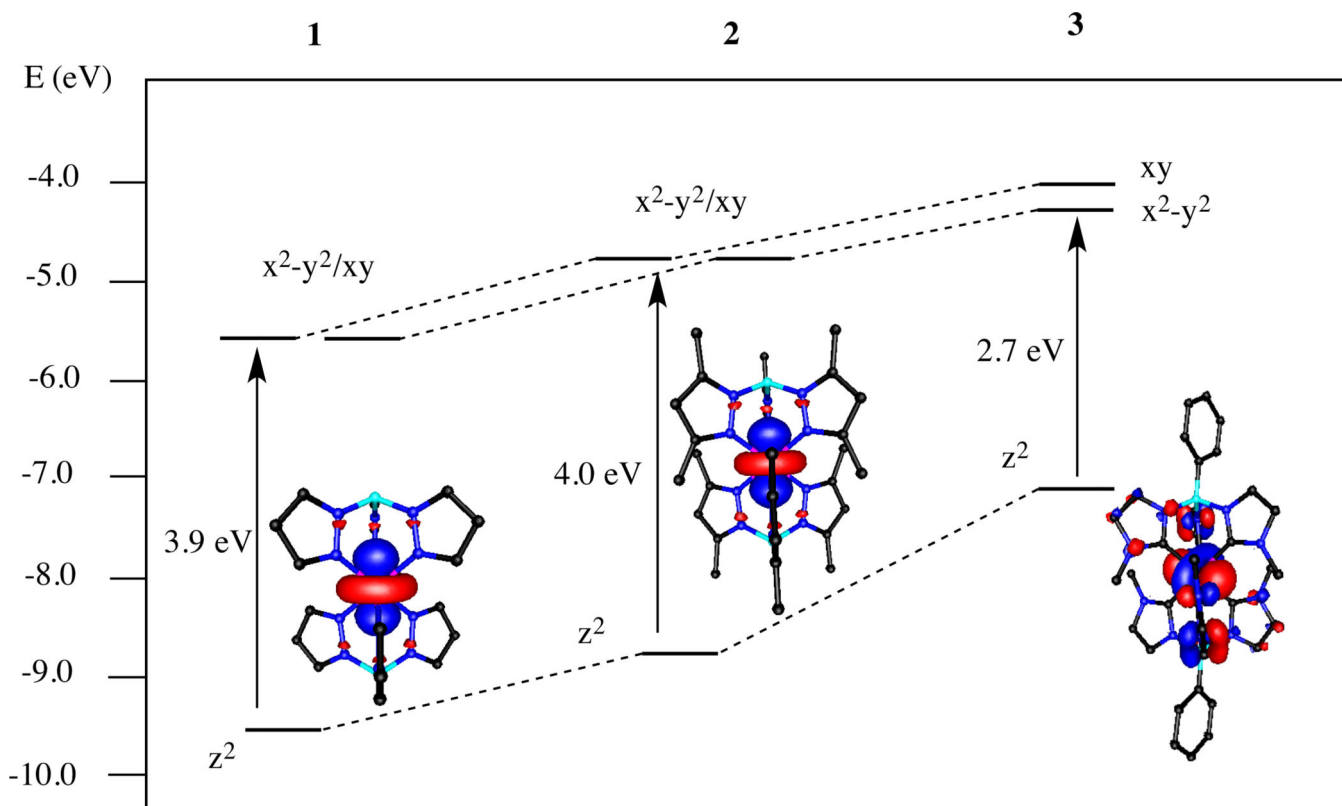|	**2**				**1**		
band	energy	polarization	assignment	band	energy	polarization	assignment
1	22 790	x,y	$^3A_2 \rightarrow$ ^3E (^{3} $_g$)	1	23 640	x,y	$^3A_2 \rightarrow$ ^3E (^3E_g)
2	23 250	x,y		2	24 500	x,y	
3	23 730	z	$^3A_2 \rightarrow$ $^3A_1$ ($^3T_{2g}$)	3	25 050	z	$^3A_2 \rightarrow$ $^3A_1$ ($^3T_{2g}$)
4	25 270	z	$^3A_2 \rightarrow$ $^3A_1$ ($^3A_{1g}$)	4	26 000[b]	x,y	$^3A_2 \rightarrow$ ^3E ($^3T_{2g}$)
5	27 530	z	c	5	25 950		$^3A_2 \rightarrow$ $^3A_1$ ($^3A_{1g}$)
6	29 980	x,y	$^3A_2 \rightarrow$ ^3E ($^3T_{2g}$)	6	28 870	x,y	$^3A_2 \rightarrow$ ^3E ($^3T_{2g}$)
				7	32 000		B-term

[a] Because of the complex appearance and variable-temperature behavior of the MCD spectra of **1** and **2**, band energies are based on the observed maxima of the MCD features rather than being obtained through a Gaussian deconvolution.

[b] The position of this band is poorly-defined.

[c] The assignment for this band is uncertain.

Table 2

CASSCF/NEVPT2-Calculated Electronic Transitions Energies (cm^{-1}) for **1**, **2**, and **3**, and MCD Band Energies for **1** and **2**.

Transition	CASSCF/NEVPT2			MCD[a]	
	1	**2**	**3**	**1**	**2**
$^3A_2 \rightarrow {}^3E\ (^3T_{1g})$	4 200	4 400	980		
	4 380	4 490	1 100		
$^3A_2 \rightarrow {}^5E\ (^5E_g)$	4 400	3 800	14 180		
	4 920	4 220	15 580		
$^3A_2 \rightarrow {}^3E\ (^3E_g)$	24 250	23 140	33 550	23 640	22 790
	24 950	24 190	34 480	24 500	23 250
$^3A_2 \rightarrow {}^3A_1\ (^3T_{2g})$	25 180	24 350	34 520	25 050	23 730
$^3A_2 \rightarrow {}^3E\ (^3T_{2g})$	25 380	24 860	34 520	26 000	29 980
	25 670	25 090	35 280	28 870	
$^3A_2 \rightarrow {}^3A_1\ (^3A_{1g})$	27 020	26 420	35 500	25 950	25 270
$^3A_2 \rightarrow {}^3A_2\ (^3A_{2g})$	27 880	27 280	36 230		
$^3A_2 \rightarrow {}^5A_1\ (^5T_{2g})$	28 920	27 390	51 140		
$^3A_2 \rightarrow {}^5E\ (^5T_{2g})$	29 200	27 470	51 420		
	33 450	32 450	52 990		

[a]The MCD energies given here correspond to the observed band maxima in the 8 K, 7 T spectra. Because the MCD spectra reflect the overlap of a large number of electronic transitions with different signs and temperature-dependent intensities, the energies of the band maxima could very well be different than the energies of the electronic transitions.

Table 3

Experimental, and Calculated Zero Field Splitting Parameters for **1**, **2**, and **3**[a]

	Experimental[b]			CP-DFT[b]			CASSF/NEVPT2		
	1	**2**	**3**	**1**	**2**	**3**	**1**	**2**	**3**
D	17.97	15.89	−49.90	10.78	9.42	8.26	16.30	14.33	37.11
E/D	0.023	0.003	0.040	0.004	0.001	0.045	0.020	0.014	0.042
E	0.42	0.04	2.00	0.042	0.016	0.371	0.324	0.200	1.56

[a] D and E values are in cm^{-1}.

[b] Experimental and CP-DFT-computed ZFS parameters were taken from reference 10. These previously reported CP-DFT calculations revealed that D is dominated by the spin-orbit coupling component (DSOC), which accounted for $90 - 95\%$ of the overall magnitude. The spin-spin coupling component (DSSC) contributes the remainder.

Table 4

DFT-calculated Percent Contributions and Orbital Energies (eV) to Selected Frontier MOs of **1**, **2**, and **3**.

| | $3d_z^2$ [a] | | | | $3d_{x^2-y^2}$ [a] | | | | $3d_{xy}$ [a] | | |
	MO	energy	% Mn	% L[b]	MO	energy	% Mn	% L[b]	MO	energy	% Mn	% L[b]
1	121β	−9.5	93	4	122β	−5.6	70	26	123β	−5.6	70	26
2	169β	−8.8	93	3	170β	−4.8	71	24	171β	−4.8	72	23
3	185β	−7.1	75	11	186β	−4.4	55	30	187β	−4.0	72	18

[a] Mn^{III} $3d_{x^2-y^2}$ and $3d_{xy}$ orbitals are the highest-energy, singly-occupied molecular orbitals.

[b] Ligand orbitals are the sum of the pyrazolyl carbon and nitrogen atoms for **1** and **2** and the sum of the N–C–N moiety for **3**.